Electrification-Ready Tribology: Experimental and Simulation Insights into Wear and Performance of Surface Optimized Valve Plates

Roman Ivantysyn[1], Ahmed Shorbagy[1], Prof. Dr. Jürgen Weber[1], Raghavendra Reddy, Reddy Reddy[2], Mathias Rauschenberger[2], Torsten Schmidt[3]

1) *TU Dresden, Institute of Mechatronic Engineering, Helmholzstrasse 7a, 01069 Dresden, Germany roman.ivantysyn@tu-dresden.de*
2) *Inline Hydraulik GmbH, 12277 Berlin, Germany, R.Reddy@inlinehydraulik.com*
3) *Fraunhofer IWU, Reichenhainer Straße 88, 09126 Chemnitz, Germany, torsten.schmidt@iwu.fraunhofer.de*

Abstract.

Axial piston pumps in electrified, variable-speed duty cycles increasingly operate at low speed and start–stop conditions where hydrodynamic lubrication margins are reduced, making the cylinder block/valve plate interface especially wear-critical. In this study, a previously optimized bronze meso-structured (sinusoidal) valve plate is re-evaluated under thermal steady-state conditions on the TU Dresden test rig at 40 °C and 60 °C inlet temperature, including very low-speed operation. The bronze design retains its efficiency benefit across both temperatures and shows no measurable additional wear, with surface changes remaining below 1 µm. Motivated by this wear-free behavior, a lead-free steel/steel material pairing is pursued. A new steel wave pattern is obtained by repeating the THED simulation optimization for the updated material pairing and was consequently manufactured and tested. Experimental results show strong efficiency improvements compared to reference and bronze configurations, but also reveal that at elevated temperature short contact events can rapidly escalate into failure. The findings confirm that meso-structured valve plates can be designed predictively for a given material system, additional research is needed to combine them with steel/steel pairings.

Keywords. Surface-structure, lead-free material pairing, electrification, axial piston pumps, valve plate, THED gap simulation.

1. Introduction

Positive displacement machines remain key components in fluid power systems due to their high power density and suitability for high-pressure operation. Axial piston pumps are widely used because of their high efficiency, variable displacement capability, and compactness as well as robustness in most heavy duty industrial applications. The ongoing shift toward electrified drivetrains has altered operating profiles. Frequent start-stop events, extended partial-load phases, and operation at low shaft speeds are increasingly required, while simultaneously high efficiency and reduced noise are expected. Under such conditions, the hydrodynamic lubrication margins of the major tribological interfaces are reduced and mixed lubrication or local contact is more likely to occur, particularly at the cylinder block/valve plate interface, which is spring pre-loaded for high speed performance, further increasing bearing loads at low-speed conditions.

In parallel, regulatory and sustainability-driven constraints have intensified the transition toward lead-free materials. In conventional pump designs, lead-containing alloys and coatings have been used to support run-in and to tolerate occasional metal-to-metal contact during early life and adverse operating points. It has been shown that surface shaping and meso-structuring can be applied to actively manipulate the lubricant film, increase hydrodynamic support, and reduce both friction and leakage losses, especially in low-speed regimes. Previous research has demonstrated efficiency gains from wave-shaped hydrostatic bearings as well as a significant reduction in wear [1], [2], [3], [4].

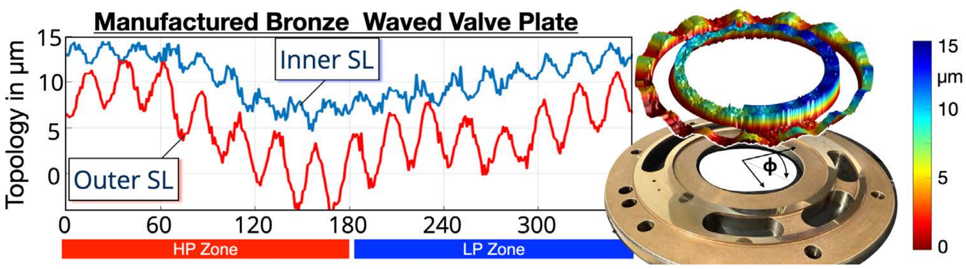

Figure 1.1. Manufactured and tested waved bronze valve plate [5].

In prior work, a meso-structured valve plate was designed using a thermo-elastohydrodynamic gap model in Caspar FSTI and was validated experimentally on an industrial test bench. A strong reduction in power losses (η_{total} +7%) at low speed was measured while high efficiency at nominal operating points was retained (η_{total} >90%). Importantly, the wave structure remained intact after testing, and the run-in behavior typical of conventional designs was substantially reduced to remain below 1 µm total wear [5].

The present contribution extends the prior work in two directions. First, repeated measurements of the bronze meso-structured valve plate were performed under thermal steady-state conditions on the TU Dresden test rig at 40 °C and 60 °C inlet temperature, including very low-speed operation (<10 rpm), to confirm performance and wear behavior under controlled thermal boundary conditions. Second, the demonstrated low-wear behavior was used to motivate a next material step toward steel/steel pairings to avoid leaded materials and to reduce dependence on costly bronze/brass materials. Since the deformation behavior and lubrication conditions differ substantially with material pairing, a new micro-structure was designed by repeating the simulation optimization for steel/steel.

2. RESEARCH GOAL

The goal of this work is to validate and extend meso-structured valve plate technology for variable-speed axial piston pumps in a way that supports lead-free and cost-effective material strategies. Two specific objectives were pursued:

1. **Confirm improved thermal stability of the waved valve plate**: Simulation results indicated that the meso-structured valve plate experiences a superior thermal response when experiencing hotter fluid temperatures. In the industrial tests the fluid temperature was not maintained steady, not allowing for a definitive validation of this claim. Hence, these tests were repeated on a research test-rig at **40˚C and 60˚C inlet temperatures**, allowing for full thermal stability.
2. **Material transition and redesign for steel/steel**: Based on the wear-free behavior of the bronze design, a transition toward a **steel/steel** pairing was to be evaluated as a next step toward lead-free and cost-relevant pump development. Due to differences in material properties a new wave pattern had to be designed using the same simulation method as published previously [5], but with an updated material pairing. Prototype manufacturing and testing were to be performed to identify performance potential and limiting failure mechanisms.

3. TEST RIG AND MEASUREMENT METHODOLOGY

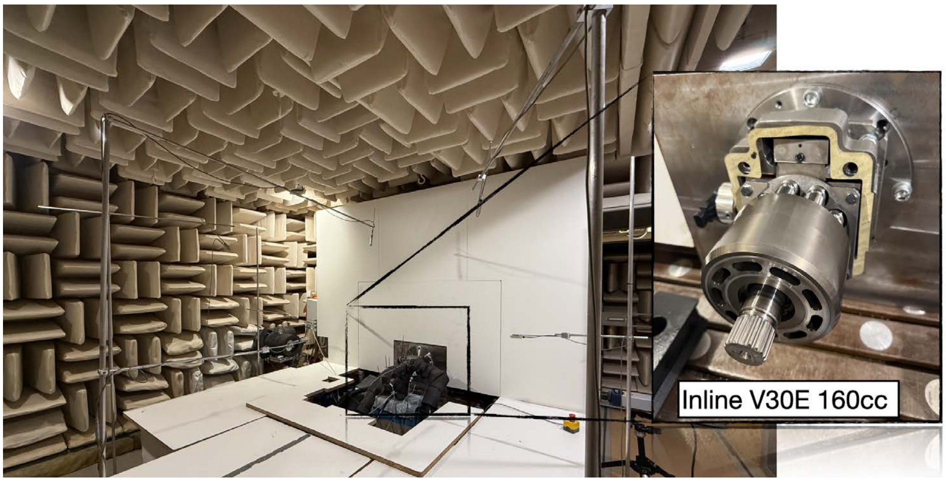

Figure 3.2. Test rig and 160cc test pump

The measurements for this work were performed in the pump test rig of the Institute of Fluid-Mechatronical Systems. This 250 kW test rig doubles as the anechoic sound measurement room, which is shown in Figure 3.2.

The pump used for this research is an V30E 160cc pump from the company Inline Hydraulik (also branded as HAWE), which is a high pressure industrial open circuit variable axial piston pump.

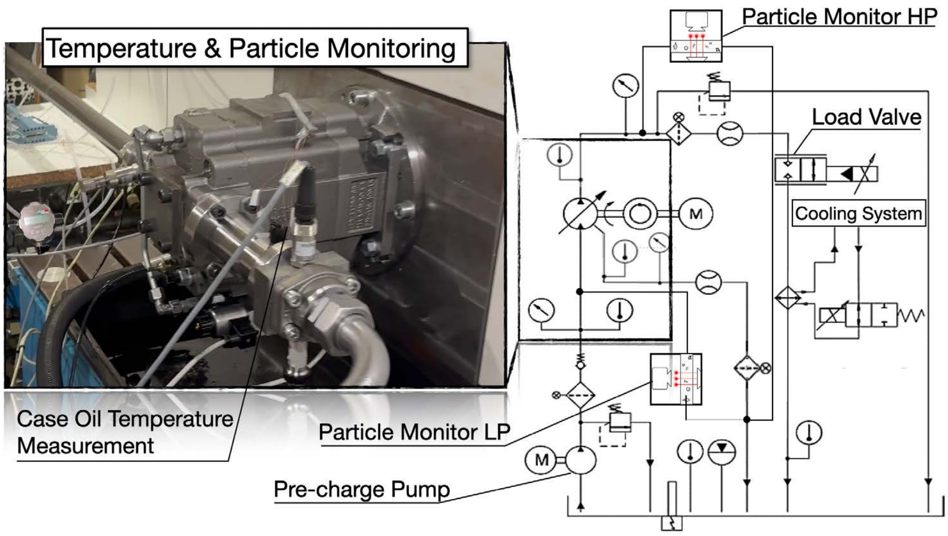

Figure 3.3. Schematic and sensor setup

The test rig features a 200 kW cooling system, capable of controlling the fluid temperature within ±1 K. In addition to the standard protocol for efficiency measurements such as pressure, temperature, flow and torque sensors, additional particle sensors as well as thermocouples were placed in strategic places (see Figure 3.3) to monitor pump performance and detect failures.

The measurement series were performed in the following order:

1. Reference measurements with a new pump (Ref1 - Kit1)
2. Repeat measurements of the used waved bronze valve plate (Bronze WVP- Kit1)
3. Unhardened waved steel valve plate (Steel WVP (S) - Kit1)
4. Hardened wave steel valve plate with a used rotating kit (Steel WVP (H) - Kit2)

The reason for the change in rotating kits, was that the unhardened steel wave had a significant failure contaminating the pump with metal particles. Hence, a rotating kit that was previously used for other measurements was used. Reference measurements were available for this replacement rotating kit, which will be compared to the Steel WVP (H) measurements only.

For each series the following measurement runs were performed:

Run1: Full operating span at 40˚C inlet
Run2: Full operating span at 60˚C inlet
Run3: Low Speed Tests
Run4: Repeat of full operating span at 40˚C inlet

Total test time: 25-30 hours.

4. PRIOR WORK AND STEADY MEASUREMENTS OF BRONZE VALVE PLATE

This paper is a continuation of the previously published meso-structured bronze valve plate [5]. This section will summarize the achievement of this paper and build upon them to lead up to the final results of the meso-structured bronze valve plate at steady state conditions.
Prior work on meso-/micro-structuring of lubricated interfaces in axial piston pumps has shown that tailored surface topographies can actively manipulate the fluid film to increase hydrodynamic load support and reduce both viscous

friction (hydromechanical) and leakage-related (volumetric) losses, especially under low-speed conditions where mixed lubrication is more likely.

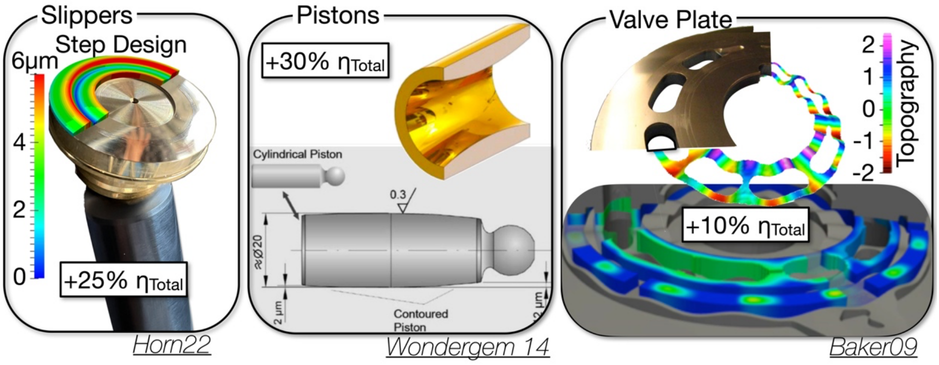

Figure 4.4. Previous published meso-structures in axial piston pumps

Across the three dominant loss-contributing interfaces—piston/cylinder, slipper/swash plate, and cylinder block/valve plate—different structure concepts and optimization targets have been published in the past and are visualized in Figure 4.4 [1], [2], [6]. The common outcome is improved low-speed efficiency with strongly reduced run-in wear when the structure is properly adapted to the interface physics. In particular, wave- or step-like meso-geometries were shown to provide measurable efficiency benefits at low speed while limiting wear to minor peak smoothing rather than bulk material removal.

Building on these findings, the present work focuses on the cylinder block/valve plate interface using the previously optimized waved bronze valve plate [5], and re-evaluates its performance under controlled *thermal steady-state* boundary conditions to remove the temperature transients inherent to the earlier industrial testing campaign.

4.1. Meso-Structured Waved Bronze Valve Plate at Steady State Conditions

Figure 4.5 summarizes the key efficiency benefit of the waved bronze valve plate at 25% displacement, showing the improvement in total efficiency (left) and the corresponding gain in hydromechanical efficiency (right) relative to the reference. The data indicate that most of the total-efficiency benefit originates from hydromechanical loss reduction, consistent with the intended mechanism of the wave structure in supporting the lubricating film. The four operating conditions used for the original design optimization are superimposed and serve as fixed reference points for later power-loss breakdowns. The choice of 25% displacement is deliberate, since valve-plate-related losses contribute a larger fraction of total losses in this regime; therefore, a ~6 percentage-point total efficiency increase (in this case from 75% to 81%) is practically meaningful.

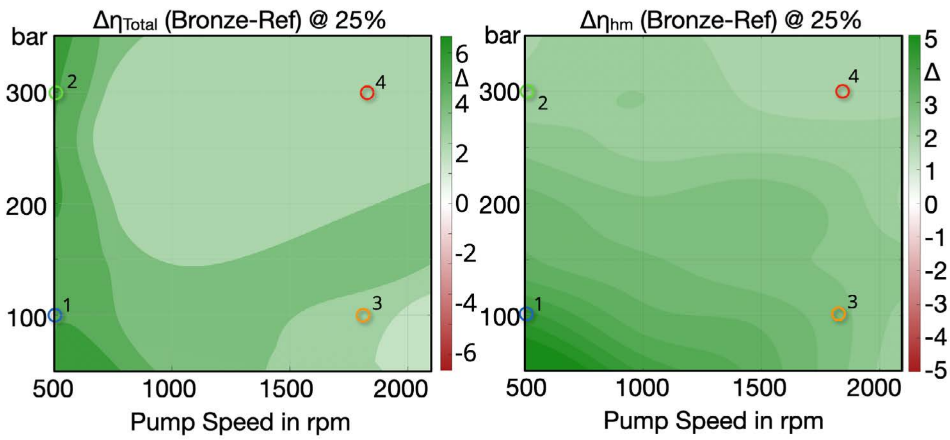

Figure 4.5. Improvement of the total and hm efficiency using a waved valve plate design in comparison to the reference at 25%

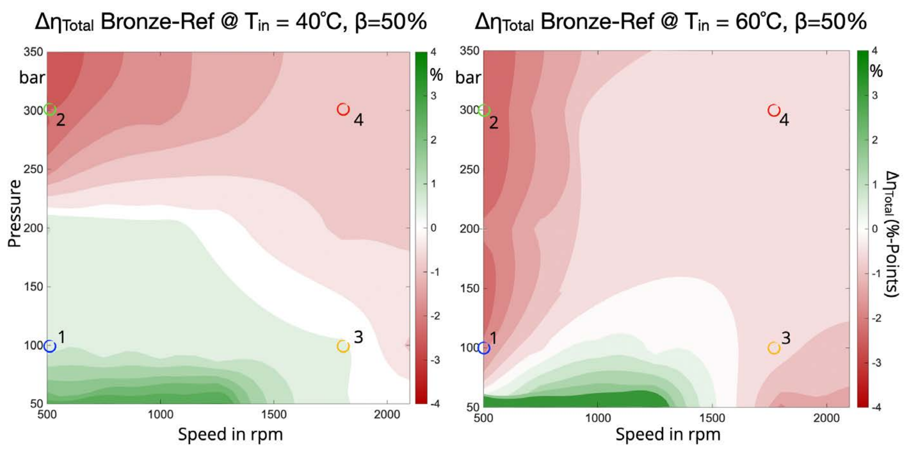

Figure 4.6. Difference between the measured total efficiency at 50% displacement for 40° and 60°C inlet temperature between the meso-structured bronze VP and the reference.

Figure 4.6 provides the measured total-efficiency difference between the waved bronze and reference valve plates at 50% displacement for two inlet temperatures. The map indicates up to ~4 percentage-point improvements

primarily at low speed and low pressure, while the majority of the operating range remains close to unchanged (approximately ±1 percentage point). A localized efficiency reduction is visible in the low-speed/high-pressure region, and the overall efficiency level decreases with increased inlet temperature, most notably at higher pressures.
To connect the efficiency trends to energy terms, Figure 4.7 shows a stacked power-loss breakdown at the four design operating conditions for the reference and waved bronze valve plates at 40°C and 60°C inlet temperature. While total losses increase at 60°C for both configurations, the waved bronze valve plate shows a smaller loss increase than the reference (~15% lower increase), supporting the simulation-based expectation that the meso-structure provides improved thermal robustness of the valve-plate interface under hotter fluid conditions.

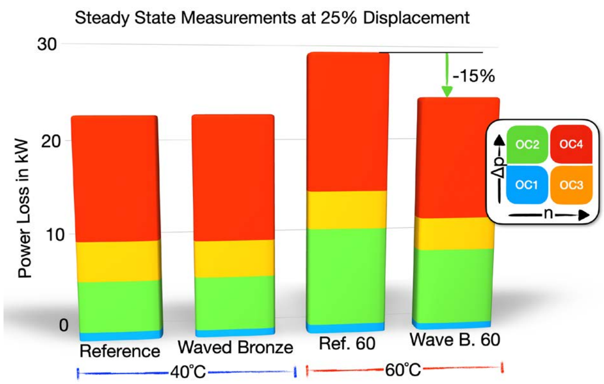

Figure 4.7. Measured efficiency improvement at 60˚C and 25% displacement across 4 main operating conditions.

This trend is further corroborated in Figure 4.8, where simulation and measurement are compared using a normalized representation: since the THED model predicts valve-plate interface losses rather than full-pump losses, values are normalized to the summed power loss at 40°C. The temperature-induced loss trend is captured well across most operating points, including a particularly strong agreement at low-speed conditions (OC1 and OC2). Deviations remain at higher-load points (notably OC3/OC4), but the agreement in both direction and magnitude is sufficient to validate the main thermal sensitivity trend relevant to variable-speed duty cycles.

In summary, the waved bronze valve plate demonstrates repeatable efficiency benefits under thermal steady-state conditions and shows a reduced loss sensitivity to elevated inlet temperature; however, the most critical requirement for long-term applicability is that the small-amplitude structure remains intact, which is assessed next via detailed wear measurements.

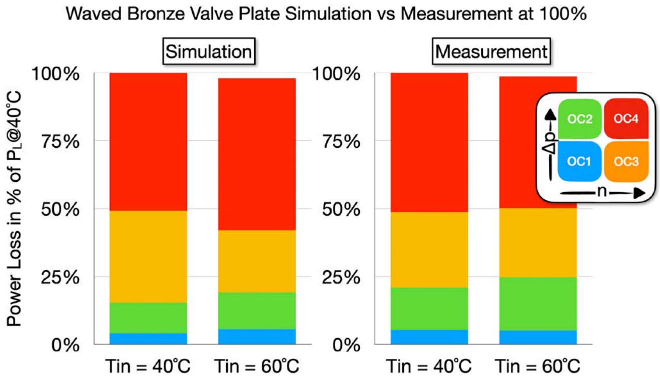

Figure 4.8. Comparison of predicted vs measured power losses at full displacement for 4 operating conditions at 40˚C and 60˚C normalized to the total power loss at 40˚C.

4.2. Evaluation of Surface Wear After Steady State Measurements

As the wave amplitudes are on the order of micrometers, even small amounts of wear can eliminate the functional hydrodynamic effect; therefore, *structure survivability* is a primary success criterion alongside efficiency. with no meaningful additional wear detected during the steady-state series.

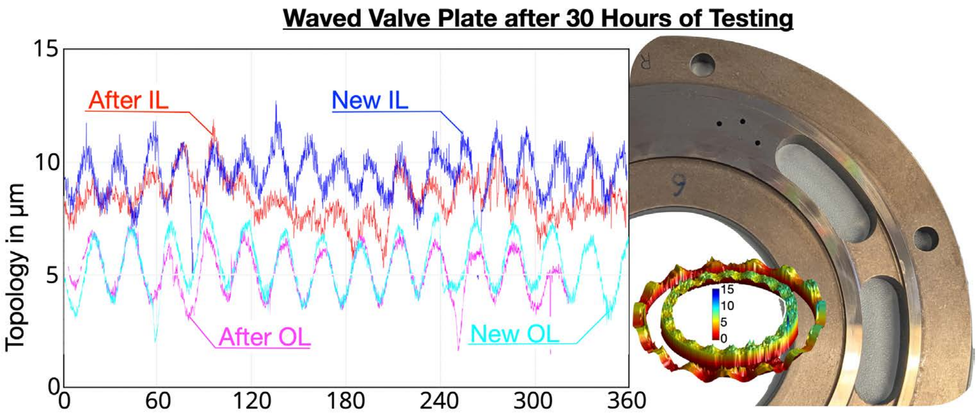

Figure 4.9. Meso-structured bronze waved valve plate new and after testing (IL = Inner sealing land; OL = Outer sealing land).

Figure 4.9 shows the waved bronze valve plate after the combined test exposure (industrial dynamic testing plus the additional steady-state campaign, totaling ~30 h). The 3D topography measurement confirms that the wave pattern remains clearly present across the sealing lands. The inner (IL) and outer (OL) sealing-land profiles, compared between the new condition and after testing, show only minor changes; while slight plastic deformation is visible—primarily at the IL—the wave form remains intact, and total material change stays below 1 µm. Importantly, the valve plate was measured after the industrial tests and again after the steady-state campaign,

The wear contrast to the reference valve plate is highlighted in Figure 4.10. Note that the color scales differ: the reference plate exhibits material loss up to approximately 5 µm at the inner sealing land and additional localized losses on the outer land, whereas the waved bronze valve plate primarily shows limited peak smoothing at the IL with the OL wave pattern largely preserved with material loss under 2 µm. Darker regions on the OL are predominantly attributable to plastic deformation rather than removal of the wave geometry, as can be seen in the surface profile in Figure 4.9.

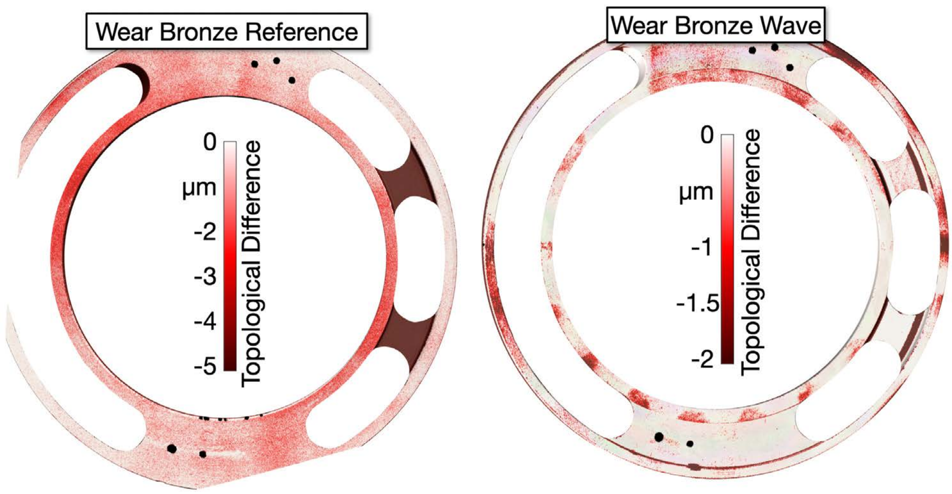

Figure 4.10. Material loss of both vale plates after industrial and steady state testing as compared to the new state.

In summary, the waved bronze concept not only improves partial load efficiency but also suppresses run-in wear to the micrometer level, motivating the hypothesis that a lead-free, cost-relevant steel/steel pairing could be feasible—provided the wave geometry is re-optimized for the fundamentally different material and deformation behavior; the following section therefore describes the simulation-based redesign workflow for steel/steel.

5. STEEL/STEEL SIMULATION AND OPTIMIZATION

The valve plate design simulations were performed within the Caspar FSTI framework, which is a powerful simulation software tailored for gap design in axial piston pumps [7]. The used model of the pump was described in detail here [5], [8], [9], [10] and validated using temperature measurements of the cylinder block [8], [9], [11].

The meso-structured wave geometry discussed in Section 4 was originally designed for the bronze WVP configuration used in the previous study. Importantly, this component is not a monolithic bronze part, but a bi-metal configuration in which the valve plate body is predominantly steel with a bronze bearing layer (~0.5mm). This material pairing influences the thermo-elastic deformation response of the valve plate: the two materials exhibit different thermal expansion behavior and stiffness, such that the resulting thermal crowning and local gap shape can differ significantly from a full steel/steel pairing. Consequently, a wave pattern that is optimal for the bi-metal configuration cannot be assumed to remain optimal—or even stable—when transferred to a monolithic steel valve plate.

To evaluate whether the bronze-derived wave concept can be transferred with minimal redesign, two parametric studies were performed on a full steel valve plate by varying only the sealing-land radii (i.e., the hydrostatic bearing area), while keeping the kidney geometry unchanged. The inner sealing land diameter was varied from d_{GapIn} = 87.5 to 89 mm and the outer sealing land diameter from d_{GapOut} = 125.5 to 128 mm, and the four previously introduced design operating conditions (OC1–OC4) were simulated in a full DOE. In the first study, a *positive-wave* pattern (IL+1 µm with +5µm offset; OL+3µm) was used, as this was the optimal design found for the bronze VP [5]. The positive wave is essentially the full wave without the negative amplitude. In a second study the full-wave pattern (IL±1 µm with +5µm offset; OL±3 µm, see Figure 1.1) was also analyzed on the steel VP. This full wave pattern reflects the realized waved bronze VP, which was chosen due to manufacturing limitations.

Figure 5.11 summarizes the results at T_{in}=35˚C as power-loss maps over the design-of-experiments domain for each operating condition. The color scale indicates the magnitude of predicted power losses (note that the scale differs between OCs), while grey regions denote non-converged simulations. Non-convergence occurred primarily when contact was predicted or when the cylinder block lifted off, both indicating an unstable design for the tested geometry. The results demonstrate that the majority of radius combinations fail in at least one operating condition. Only a single candidate (Des20) converged in all four OCs; however, the lowest-loss region is shifted toward smaller values of d_{GapIn} and d_{GapOut} where designs such as Des72 approached favorable loss levels but still failed to converge in OC4. As a reference the bronze WVP had 88.5mm and 127.4 mm as d_{GapIn} and d_{GapOut} respectively. Nevertheless, both Des72 and Des20 showed problems at 60˚C inlet, a temperature when the full wave pattern was superior.

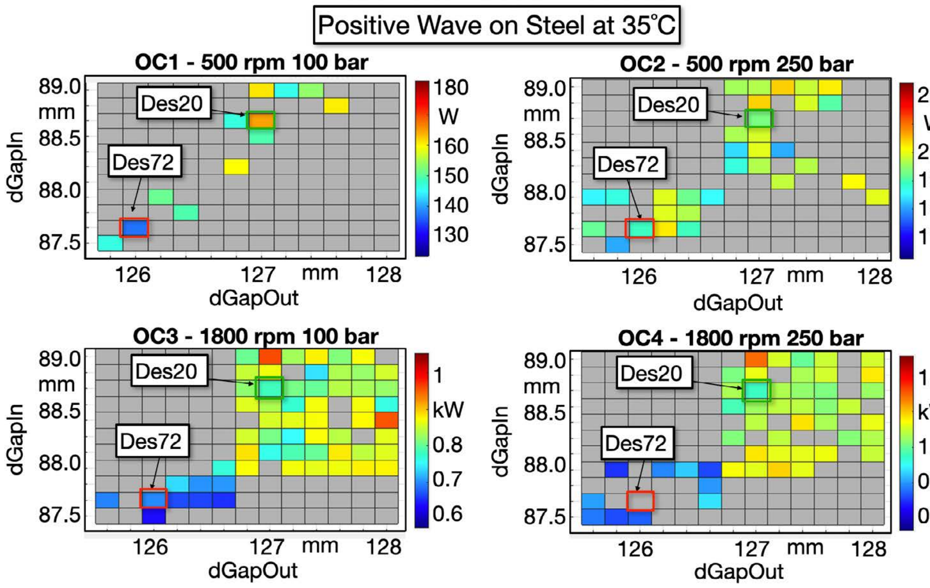

Figure 5.11. Powerlosses with variation of the sealing land width on a steel VP for a positive wave design adapted from the waved bronze VP

The results of the full wave pattern at T_{in}=35˚C are shown in Figure 5.12. While the loss levels were, on average, reduced compared with the positive-wave sweep, the same fundamental limitation remained: only one design converged across all four OCs, and the best-performing low-loss candidate (Des33) still failed in OC4. This indicated that the stability margin of the hydrostatic balance in steel/steel is highly sensitive and that “best loss” and “robust across OCs” do not coincide when only the sealing-land radii are varied. Des 33 converged in all OCs at 60˚C inlet temperature, making it the base for further amplitude studies.

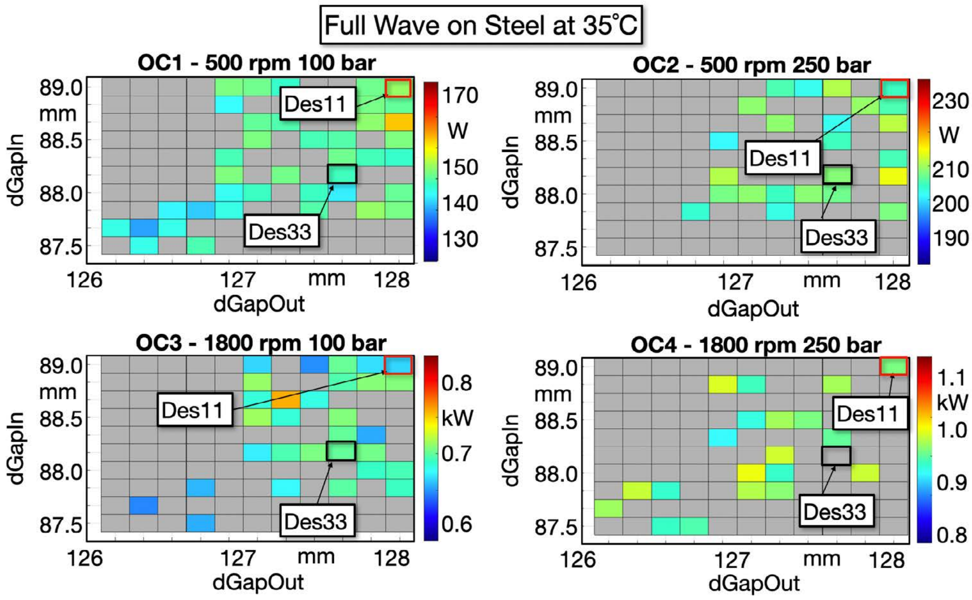

Figure 5.12. Powerlosses with variation of the sealing land width on a full steel VP for a full wave design adapted from the waved bronze VP

Since the bronze steady-state measurements in Section 4 revealed a strong temperature dependence, both geometrical studies were repeated at an elevated inlet temperature of $T_{in} = 60^{\circ}C$. The outcome was a qualitative change in behavior: the formerly robust positive-wave candidate (Des20) failed at higher temperature (already in OC3), whereas Des33 became stable and exhibited very low predicted losses at elevated temperature.

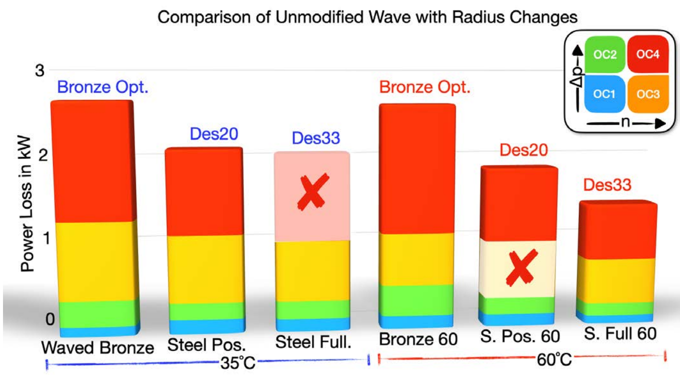

Figure 5.13. Direct adaption of full and positive wave from bronze design to a steel VP adjusting the sealing land width only.

Figure 5.13 condenses these findings by comparing stacked valve-plate power losses over the four operating conditions for essentially the same wave pattern, only (differentiating between positive and full wave) for the bronze and steel VP at inlet temperatures of 35°C and 60°C. While the steel VP can, in principle, achieve lower valve-plate losses than the bronze design at both temperatures, none of the directly transferred configurations provided a single radius choice that remained stable and convergent across all four operating conditions and both inlet temperatures. In other words, the transfer produced attractive "point solutions," but no robust design envelope.

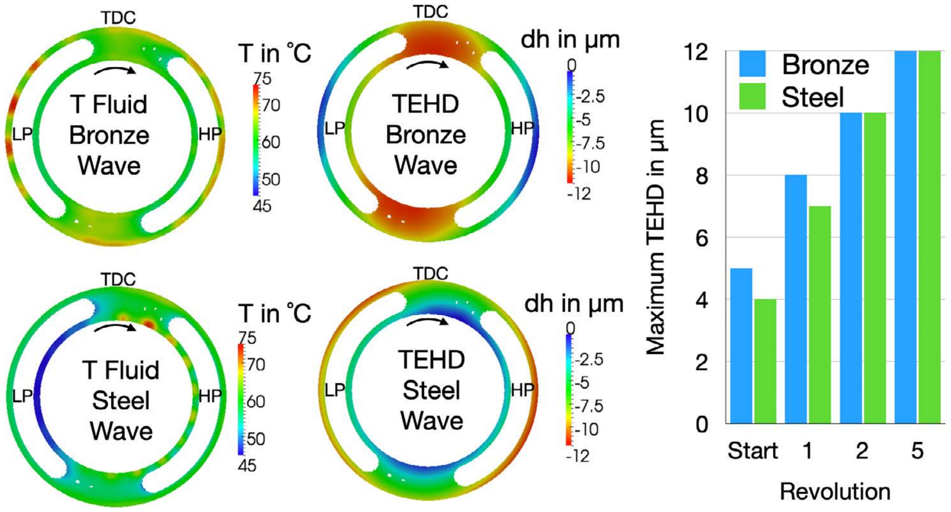

Figure 5.14. Thermal deformation effect on the fluid film between bronze and steel waved valve plate at OC4 (1800 rpm, 300bar, 100%)

The underlying cause of this temperature-dependent instability is the fundamentally different thermo-elastic deformation pattern of the full steel VP compared with the bi-metal bronze configuration. This is illustrated in Figure 5.14 for OC4, where the simulated fluid-film temperature distribution (left) and the gap-height change caused by thermo-hydrostatic-elastic deformation (THED contribution shown in the middle) are shown for both material systems. Although the *magnitude* of thermal deformation is comparable, the *spatial distribution* differs drastically: the bi-metal configuration produces a deformation pattern that creates a low spot in regions between the HP and LP kidney around TDC/BDC, whereas the full steel VP experiences the highest points in these critical areas. Because the wave pattern is designed to interact constructively with the thermo-elastic deformations, this shift explains why a geometry optimized for the bi-metal plate can become unstable when applied to steel/steel—particularly at OC4, where thermal gradients and pressure loading are most severe.

On the right side of the figure is the maximum THED of the valve plate with the simulation revolution. The simulation framework calculates the thermal conditions after each completed revolution and updates the thermal boundary conditions; thus, each revolution is associated with a modified thermal deformation field. When a design completes the first 3 revolutions and then fails, it is usually due to thermal deformations. This will be relevant later in this section.

As the direct adaptation of the bronze wave pattern onto the steel VP was shown to be unwise, a new wave optimization was performed. Due to time constraints, the optimization scope was restricted to a full-wave concept with the same phase and frequency as the bronze design, while varying predominantly the wave amplitudes and offsets. This restriction was motivated by prior sensitivity results indicating that amplitude is typically the dominant parameter, while phase and frequency have secondary influence for the bronze configuration.

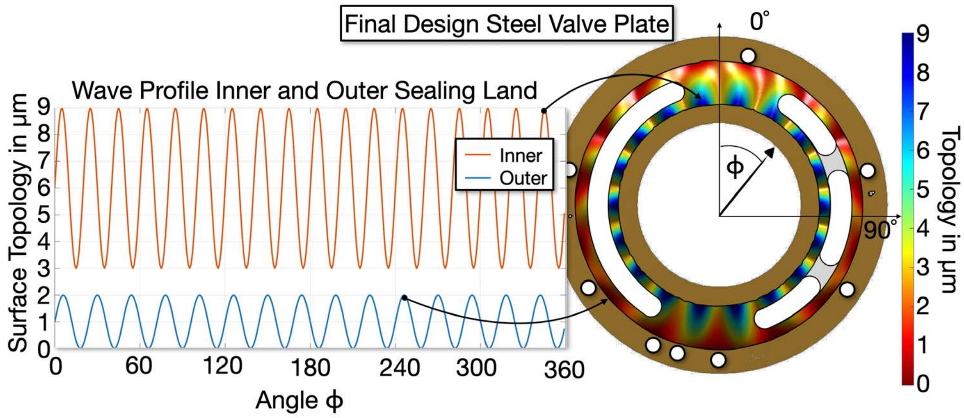

Figure 5.15. Final manufactured design for the steel valve plate with a full wave design and adapted sealing land width.

The resulting optimized steel design is shown in Figure 5.15 and differs significantly from the optimized bronze wave plate: whereas the bi-metal bronze plate used a larger outer-land amplitude (±3 µm) and a smaller inner-land amplitude (±1 µm) with a 7 µm offset, the optimized steel design essentially inverts this distribution by placing the dominant waviness on the inner sealing land (±3 with a 6 µm offset) and reducing the outer-land amplitude to ± 1µm. In addition, the steel design extends structuring across the full sealing-land circumference, including transition regions around TDC and BDC.

The performance predicted performance of this design is shown in Figure 5.16 in form of stacked power loss bars. The found design is predicted to substantially reduce power losses by more than 30% at 35°C inlet and 35% at 60°C inlet, when compared to the already well performing bronze wave design. This demonstrates the strong potential of steel/steel when the wave is designed for the correct thermo-elastic response. However, even with the redesigned wave pattern, a fully robust solution for OC4 at elevated temperature was not achieved within the limited optimization scope.

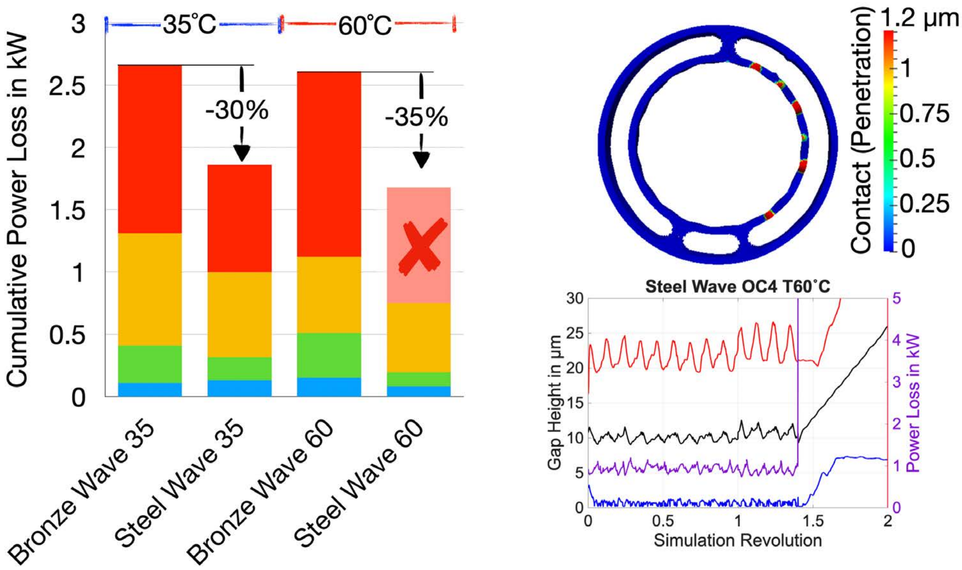

Figure 5.16. Final design steel valve plate after re-running full optimization (left). Right: Simulation result for OC4 Steel Wave 60, with predicted wear at the inner sealing land.

As shown on the right side of Figure 5.16 the steel design shows contact on the inner sealing land at OC4 at 60˚C inlet temperature. The graph on the bottom right of the figure confirms, that this is primarily due to a thermal deformation problem, as the first revolution delivered very good power losses of under 1 kW for this interface. For comparison, the standard valve plate produces about 2.4 kW power losses at this condition. However, after the simulation entered the second revolution the simulation predicted contact and crashed at the end of the high-pressure stroke. For this reason, the OC4 “result” should be interpreted as an initial-revolution indicator rather than a validated steady-state prediction, indicating that this design might experience problems at high speed, high pressure and high temperature.

Despite this remaining limitation, the significantly improved power losses and the stable behavior at 35°C across the majority of the operating domain motivated fabrication of the optimized steel valve plate to experimentally validate the low-temperature performance and to identify the limiting failure mechanisms in a controlled measurement campaign. A complete optimization over phase, frequency, amplitude distribution, offsets, and sealing-land geometry is expected to enable convergence across all operating conditions and both inlet temperatures; however, this extended design space was outside the available project timeframe. The following section therefore describes the manufacturing approach and the experimental validation of the optimized steel valve plate concept.

6. MANUFACTURING AND SURFACE MEASUREMENTS

Manufacturing of the steel meso-structured valve plates was carried out at Fraunhofer IWU (Chemnitz). IWU previously produced the step-structured slippers and the waved bronze valve plate discussed in Section 4 using precision turning, where the micro-topography is generated via a piezo-actuated tool path. For the present steel design, a laser-based structuring route was selected instead. Steel is well suited for ultrashort-pulse ablation, and the laser process offers (i) high geometric fidelity for shallow µm-scale features, (ii) flexible patterning without dedicated tooling, and (iii) robust repeatability for complex wave layouts. The applied laser setup with the resulting wave like structure is shown in Figure 6.17. It uses an femtosecond ultrashort-pulse TruMicro 2030 laser (average power: 20 W, wave length: 1030 nm, pulse rate: 300 fs–20 ps).

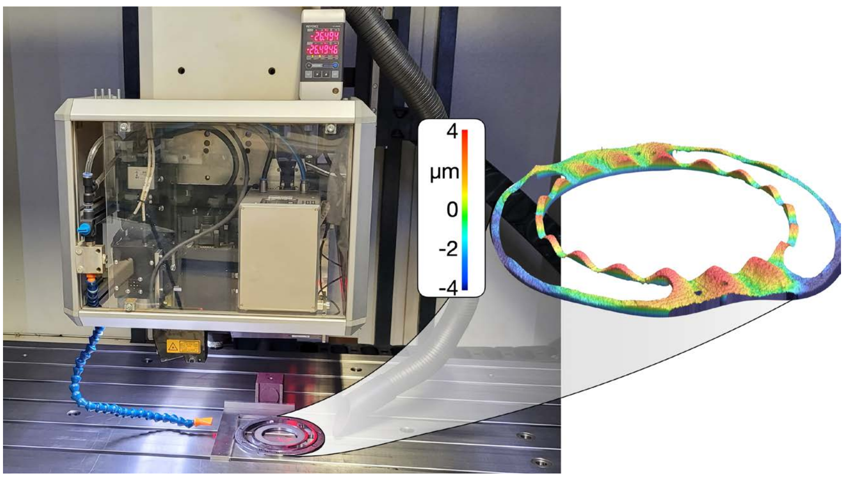

Figure 6.17. Laser structuring at the Fraunhofer IWU

A total of four steel valve plates were manufactured: two in an unhardened steel condition and two as hardened parts. The unhardened variant was intended to provide a more forgiving material response against the hardened cylinder block surface during possible mixed-lubrication events occurring at start-up or brief moments of dynamic changes. However, this assumption did not hold across the full operating envelope. In subsequent testing, the unhardened valve plates exhibited limitations at high-pressure conditions, whereas the hardened valve plates demonstrated clearly improved robustness at elevated pressures. The premature failure at high pressures motivated the focus on hardened steel valve plates for the high-pressure validation steps.
The manufactured valve plate and a superimposed 3D surface measurement are shown in Figure 6.18. The measured surface profiles on the inner land (IL) and outer land (OL) indicate that the realized wave amplitudes deviate moderately from the nominal targets: the OL is approximately ±1.5 µm (target ±1 µm), while the IL is approximately ±2.5 µm (target ±3 µm with offset). This deviation is likely influenced by the pre-existing flatness error of the valve plate prior to structuring (≈3.4 µm), which cannot be fully compensated by the laser structuring process. Nevertheless, the achieved geometry was considered acceptable, since the amplitudes remain within the tolerance band for which the simulations indicated robust performance.
Despite this deviation, the overall structure—frequency, phase relation, and relative amplitude concept—was realized consistently. The wave topographies are not visually apparent to the naked eye; instead, the structured region primarily becomes noticeable through characteristic color effects from light diffraction/reflection on the textured surface as captured in the photograph on the right.

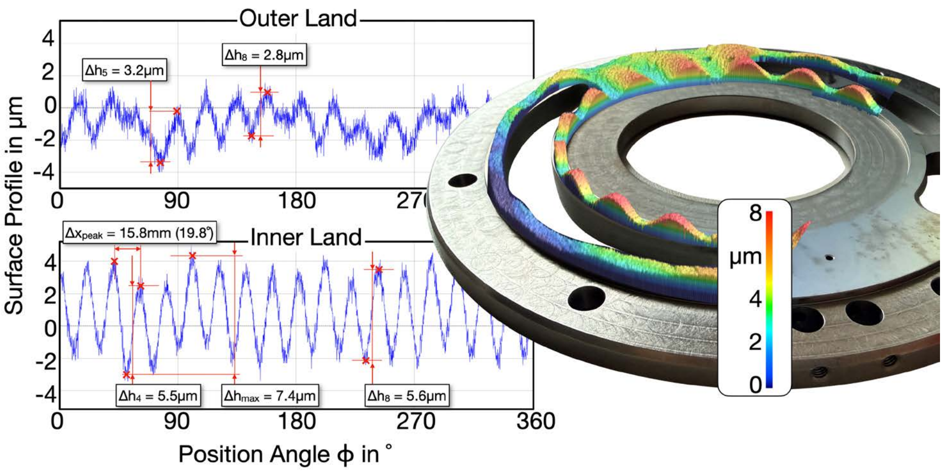

Figure 6.18. Manufactured waved full steel valve plate with surface scan.

With the steel valve plates manufactured and geometrically verified, the next section presents the experimental results for the steel/steel pairing, including performance mapping, temperature/particle monitoring, and the observed failure mechanisms under high-pressure and elevated-temperature conditions.

7. EXPERIMENTAL RESULTS: STEEL/STEEL VALVE PLATES (UNHARDENED THEN HARDENED)

Both variants of the meso-structured full-steel valve plate described in Section 6 (unhardened and hardened) were tested in the same measurement procedure described in section 3, using identical instrumentation for pressure, flow, torque, temperature and particle monitoring. The results are presented in two parts.

In Section 7.1, the unhardened steel waved valve plate (Steel WVP (S)) is directly compared against the waved bronze valve plate and the reference valve plate using **Rotating Kit 1**, for which complete reference measurements (Ref1) were available at both 40˚C and 60˚C inlet temperatures and including the low-speed measurements. Unfortunately, the unhardened steel plate failed prematurely, severely damaging the cylinder block and contaminating the pump with metallic debris, which necessitated a hardware change. Consequently, Section 7.2 focuses on the hardened steel valve plate measurements performed with a **replacement rotating kit (Kit 2)**. For Kit 2, a reference data set was available from other projects [12], but not for 60 °C and not for the ultra-low-speed conditions; furthermore, Kit 2 had already seen significant prior operation and therefore exhibits lower baseline efficiency than the new Kit 1. For this reason, the hardened steel results are evaluated primarily relative to Reference Kit 2 (Ref2) in terms of efficiency.

7.1. Rotating Kit 1 – Unhardened Steel Valve Plate

The unhardened steel wave valve plate was tested over the operating range 250–2100 rpm and 50–250 bar at 40˚C inlet temperature, before the test campaign was interrupted by a premature failure that occurred at 1800 rpm and 250 bar. Up to the onset of failure, Steel WVP (S) showed a remarkably strong efficiency potential and, in large parts of the map, outperformed both the new reference valve plate and the waved bronze valve plate—showing significant improvements even at full displacement.

Figure 7.19 summarizes this efficiency by showing the total efficiency difference of the Steel WVP (S) relative to Ref1 (left) and relative to the waved bronze valve plate (Bronze WVP) (right). The steel WVP yields pronounced gains at low speed and low-to-medium pressures, reaching +10 percentage points over the reference and up to +16 percentage points over the bronze configuration at 250 rpm and high pressure (250 bar).

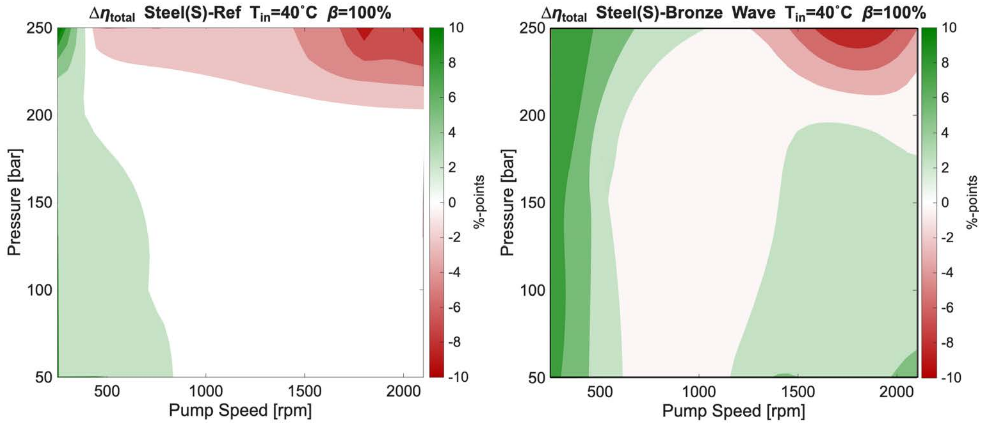

Figure 7.19. Efficiency difference between the unhardened steel WVP, the reference Kit1 and the bronze WVP at 40˚C inlet and 100% displacement

In the low-pressure region the advantage persists up to roughly 750 rpm, after which the performance approaches the reference level. At higher pressures, the efficiency initially remains improved but then degrades rapidly as the operating point approaches the failure region; immediately before failure, a strong drop is observed at high speed and 250 bar. Despite the failure, the magnitude of the low-speed improvement is significant. Increasing the total efficiency from 61% to 76% at 250 rpm, 250 bar and full displacement represents a substantial step toward electrification-relevant operating conditions, and the improvement over the already optimized waved bronze valve plate at low speed and high pressure indicates that the steel-specific wave interaction and thermal-mechanical behavior can produce different—and in parts more favorable—trends than the bronze-based design.

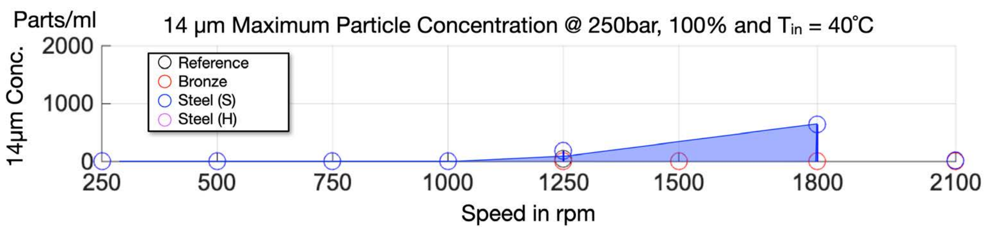

Figure 7.20. Maximum 14µm particle production at 250bar and 40˚C

Figure 7.20 shows the maximum concentration of 14 µm particles in the HP line at 250 bar and T_{in} = 40 °C for all tested valve plates. While Ref1 and the bronze WVP remain at low particle levels, Steel WVP (S) begins producing large particles already at 1250 rpm, and the particle concentration increases dramatically until the full failure at 1800 rpm. Notably the Steel WVP (H) did not produce any particles at this temperature and pressure. The resulting damage state is documented in Figure 7.21, where both the valve plate and the cylinder block exhibit severe wear, with grooves exceeding 0.5 mm in depth.

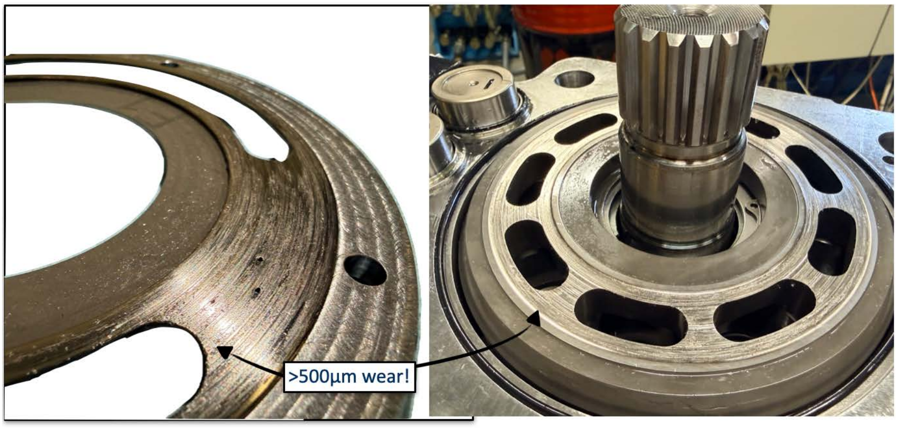

Figure 7.21. Failure of the unhardened steel valve plate after reaching 1800rpm and 250 bar at 40˚C.

This outcome highlights an important characteristic of steel/steel pairings: they are highly unforgiving once mixed lubrication and local contact occur. The meso-structure operates at the micrometer scale and is therefore sensitive to early damage. Moreover, the steel valve plate geometry was intentionally adapted (reduced sealing land width) to compensate for the additional hydrodynamic lift of the wave. Once wear occurs it removes or damages the meso-wave structure. After losing the additional hydrodynamic lift and the interface became critically underbalanced, accelerating contact, heat generation, and material removal. Post-test inspection further indicated plastic deformation of the unhardened plate, indicating that the high pressure loading deformed the VP, which is an effect that the simulation model cannot capture as only elastic deformation is considered.

These findings motivated the second steel configuration: a hardened wave valve plate intended to provide higher resistance against pressure-driven deformation and to improve robustness under the high-pressure operating points. The following Section 7.2 therefore evaluates the hardened steel wave valve plate using Rotating Kit 2 and compares its efficiency performance to the corresponding reference for that kit.

7.2. Rotating Kit2 – Hardened Steel Valve Plate

The hardened steel waved valve plate (Steel WVP (H)) was tested with rotating kit 2 and is therefore evaluated exclusively against the corresponding reference measurement of kit 2 (Ref2). Figure 7.22 summarizes the resulting efficiency differences at 100% and 50% displacement. The largest gains occur at low pressure and in the operating regions that are most relevant for variable-speed duty cycles: at 100% displacement the total efficiency increases by more than 7 percentage points around 1000 rpm (from 80% to 87%), while at 50% displacement improvements of roughly 5 percentage points are observed at high speed (at 1800–2100 rpm from 70% to 75%). Importantly, these benefits are achieved with only minor efficiency drawbacks at high pressure and low-speed, where the efficiency decreases by approximately one percentage point.

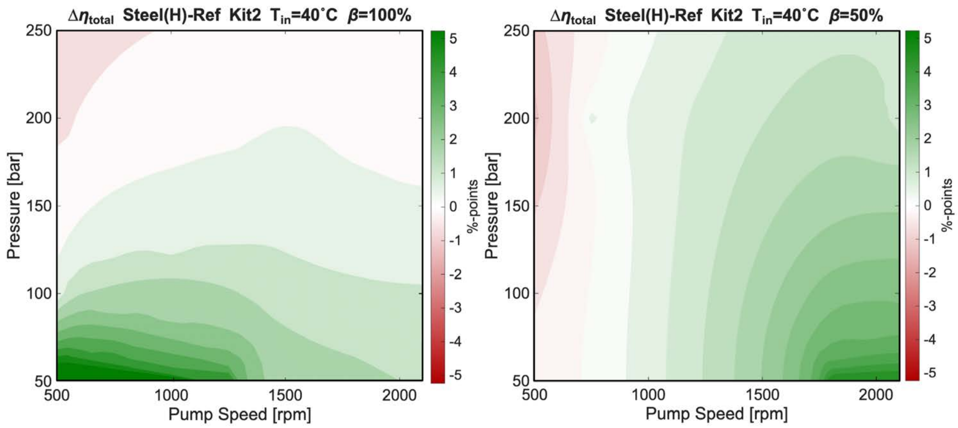

Figure 7.22. Efficiency difference between the hardened steel WVP and the reference for rotating kit 2 at 100% and 50 % displacement at 40˚C inlet.

The simulation-based performance trend is thereby validated and is further reflected in the operating-condition power-loss evaluation shown in Figure 7.23. In the design phase (Figure 5.16), the thermo-elastohydrodynamic optimization predicted a substantial reduction of valve-plate interface losses, primarily at OC3 and OC4 at 40 °C inlet temperature; the predicted relative reduction of interface losses corresponds to an absolute reduction on the order of 0.7 kW. Experimentally, a reduction of 1.1 kW

(~4%) is obtained when summing OC1–OC4 at 100% displacement. At 50% displacement the reduction increases to 3.6 kW (~17%). These results confirm that meso-structures can deliver a measurable reduction in losses even in a steel/steel pairing and across a wide speed range—an essential prerequisite for electrification-ready pump concepts where the machine is frequently operated in various speed domains.

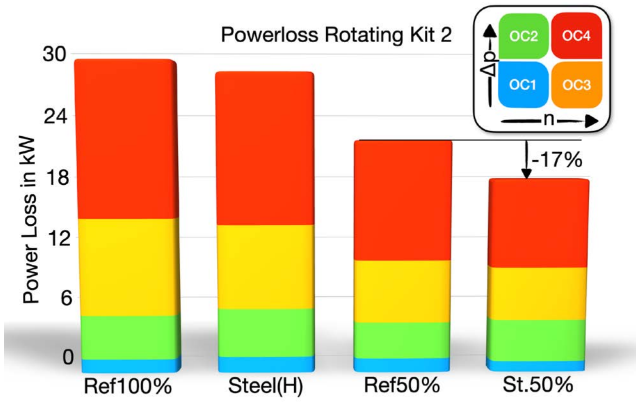

Figure 7.23. Efficiency improvements of the hardened steel VP at 100 and 50% at 40˚C inlet temperature for OC1-4.

Besides efficiency, the key system-level metric for electrified drives is torque demand, because required motor size, peak current capability, and thermal load scale directly with torque.

Figure 7.24 therefore compares torque losses at 50 bar and 200 bar. Due to the premature failure of the first steel valve plate and the lack of low-speed reference measurements for Kit 2, the comparison necessarily combines data from both rotating kits. As expected, Kit 1 exhibits lower torque losses overall, consistent with its higher efficiency baseline. Nevertheless, Steel WVP (H) (Kit2) shows very pronounced torque-loss reductions: at 50 bar and 20 rpm, the torque loss is reduced by approximately 66% (more than 10 Nm). By extrapolating the trend onto Kit1 (red dashed line), a further reduction is likely, amounting to 80% torque reduction when comparing the same rotating kit with each other. At 200 bar, the torque-loss reduction amounts to more than 30% at 250 rpm and remains around 20% over a broad speed range, which directly translates into a substantially reduced e-motor torque requirement and therefore offers a clear pathway to smaller and lower-cost electric drive systems.

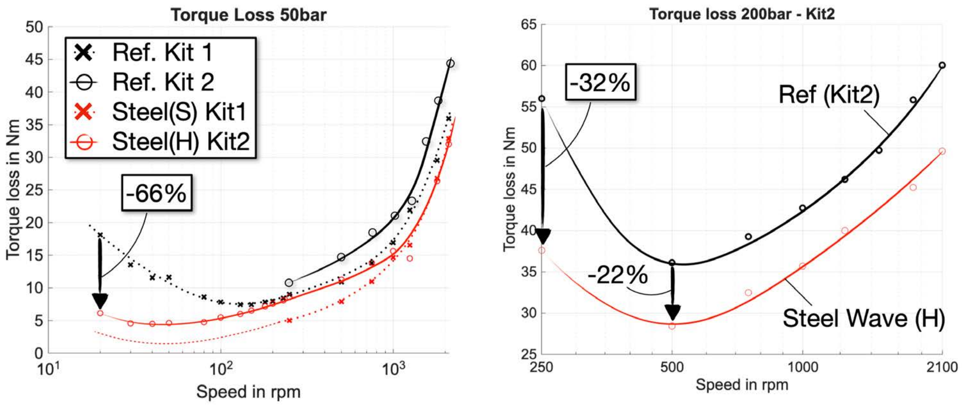

Figure 7.24. Improved low speed torque loss at 50 bar and 200bar for both rotating kits.

Up to this point, the hardened steel WVP confirms the simulation predictions and demonstrates strong potential. However, the results also confirm the key limitation of steel/steel pairings: once contact occurs under high temperature and elevated speed, wear becomes rapidly self-accelerating.

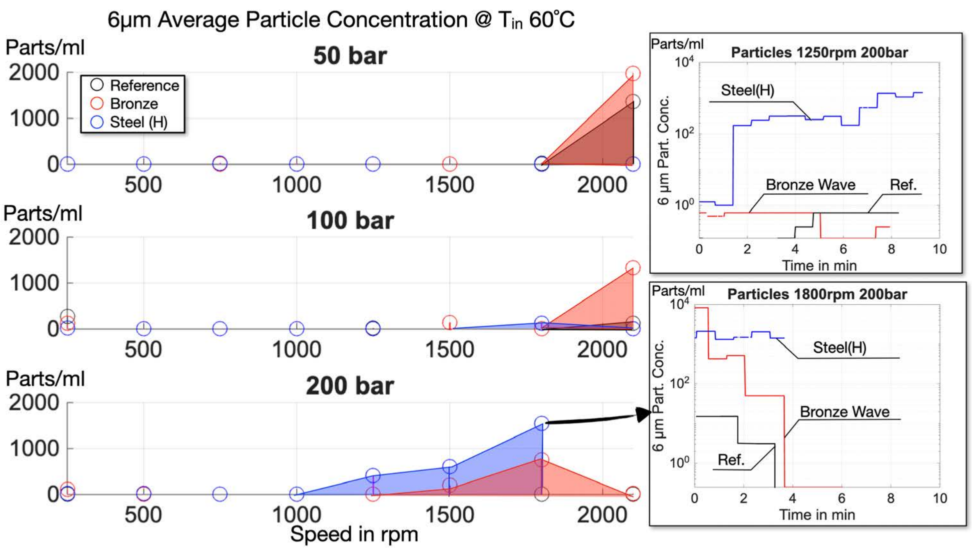

Figure 7.25. Average particle generation at 60˚C inlet temperature with zoom-ins at 1250 rpm and 1800 rpm at 200 bar.

Figure 7.25 shows the average 6 μm particle concentration in the HP-line for 60°C inlet temperature over the tested speed and pressure range. The 6 μm class is chosen because it provides two practically relevant insights. First, it acts as an early warning indicator for impending failure in steel/steel interfaces: at 1250 rpm and 200 bar the particle concentration begins to rise and remains elevated over time even though the pump is still operating with acceptable efficiency. Continuing operation leads to further escalation, and at the final operating point (1800 rpm, 200 bar) the concentration increases strongly (note the logarithmic y-axis scaling), accompanied by the emergence of larger particles, which triggered the shutdown event. Second, the same measurement highlights the robustness of bronze-based pairings during short contact events: both the reference and the bronze valve plate can show elevated particle production at high speed and high temperature (e.g., the bronze waved valve plate at 1800 rpm and 200 bar), but the particle generation typically decays back toward zero, consistent with a gentle run-in mechanism. In contrast, steel/steel contact tends to remove micrometer-scale material and generate larger fragments, leaving grooves that promote further contact and accelerate damage. Post-test inspection of Steel WVP (H) showed severe grooving and wear depths on the order of several hundred micrometers, similar to the unhardened case, indicating that once the surface structure is damaged the interface can no longer act as a controlled hydrostatic/hydrodynamic bearing. If the VP would have had a similarly forgiving tribological material pairing, then the VP would have likely survived.

8. DISCUSSION

Across both rotating kits, the experiments demonstrate that meso-structured valve plates can be designed to significantly improve efficiency and reduce torque losses in operating regions that dominate variable-speed duty cycles. The steel designs, in particular, show that a hard/hard pairing does not inherently prevent performance benefits. On the contrary, the steel material allowed for a design of an even superior wave pattern, improving efficiency by more than 10% and torque loss by 60-80%, which directly supports electrification-driven requirements for compact and efficient motor-pump units.

At the same time, the measurements expose the central robustness challenge. While bronze-based systems can tolerate brief metal-to-metal contact through a forgiving run-in mechanism with limited wear volume, steel/steel contact can rapidly transition into severe, self-amplifying wear. Particle monitoring—especially in the 6 µm class—proved to be a sensitive early indicator of such failure onset, but preventing the underlying contact remains the primary requirement for a viable steel/steel implementation.

The simulation model predicted wear at high inlet temperature and elevated pressure, which the measurement confirmed. Previous designs optimized with the Caspar FSTI suite also indicated brief wear periods, something that a soft/hard material pairing usually accepted. However, the study has shown when designing a hard/hard pairing with meso-structures, contact needs to be avoided in all operating conditions, even when just brief. With a more time and exploring a larger design space, the author is confident that a suitable design can be found.

9. CONCLUSIONS AND OUTLOOK

This study confirms that meso-structured valve plates can improve the performance of axial piston pumps operated under electrification-relevant, variable-speed conditions. The structured bronze valve plate maintains the previously reported benefits and exhibits negligible wear, even when operated at steady-state thermal boundary conditions.

Extending the same design to steel/steel interfaces was not feasible, as the bi-metal bronze valve plate experiences different thermal expansion as a full steel one. Hence, a complete redesign had to be performed, yielding very different sealing land structures. The steel wave valve plate demonstrated even larger improvements in efficiency and torque demand, indicating that meso-structures can support lead-free and cost-relevant material strategies.

However, the steel/steel results also highlight that robustness, not peak efficiency, is the limiting factor. Once contact occurs at elevated temperature and speed, steel/steel interfaces can rapidly generate large wear volumes, destroy the micro-structure, and lose the hydrodynamic and hydrostatic balancing on which the design is based. Future work should therefore focus on mechanisms that allow short contact events without catastrophic damage, while simultaneously exploring a larger design space to avoid contact even at the most extreme conditions.

When combining these measured findings of over 80% torque reduction and 10-30% efficiency improvements, with the similarly impressive meso-structured slippers published in previous research [4], it becomes clear, that pump designs can be significantly improved when combining surface structures to all hydrostatic bearings. With these additions, meso-structuring offers a high-potential pathway to electrification-ready, lead-free axial piston pump designs that combine efficiency gains with reliable long-term durability.

ACKNOWLEDGEMENTS

The authors would like to thank Inline Hydraulik GmbH and the Fraunhofer IWU for supporting this research with donations and services. Without their kind support this research would have not been possible.

10. REFERENCES

[1] M. Ivantysynova and J. Baker, "Power loss in the lubricating gap between cylinder block and valve plate of swash plate type axial piston machines," *International Journal of Fluid Power*, vol. 10, no. 2, pp. 29–43, 2009, doi: 10.1080/14399776.2009.10780976.

[2] A. M. Wondergem, "Piston/Cylinder Interface of Axial Piston Machines - Effect of Piston-Micro Surface Shaping," 2014. doi: 1585442.

[3] A. A. Darbani, L. Shang, J. R. Beale, and M. Ivantysynova, "Slipper surface geometry optimization of the slipper/swashplate interface of swashplate-type axial piston machines," *International Journal of Fluid Power*, vol. 20, no. 2, pp. 245–270, 2019, doi: 10.13052/ijfp1439-9776.2025.

[4] R. Ivantysyn, S. Horn, and J. Weber, "Design of a Lead-Free Slipper Bearing for Low Speed Axial Piston Pump Applications," *International Journal of Fluid Power*, vol. 25, no. 2, pp. 183–202, 2024, doi: 10.13052/ijfp1439-9776.2524.

[5] R. Reddy, R. Ivantysyn, and P. J. Weber, "Advanded micro-surfacing: Tribological optimization for variable speed hydraulic drives," in *ASME/BATH 2025 Symposium on Fluid Power and Motion Control, FPMC 2025*, 2025, pp. 1–15.

[6] S. Horn, R. Ivantysyn, and J. Weber, "Tribo-optimized lubricating interfaces in hydrostatic pumps with surface shaped slippers," in *IFK2022*, Aachen, 2022.

[7] SHS GmbH, "Caspar FSTI The most powerful axial piston pump model." [Online]. Available: https://www.smart-hydraulic-solutions.com/casparfsti

[8] R. Ivantysyn and J. Weber, "Thermal Insights and Predictive Modeling of Axial Piston Pumps : A Journey to a High-Fidelity Digital Twin," in *Maha Conference 2024*, 2024, pp. 1–19.

[9] R. Ivantysyn, A. Shorbagy, A. Vedpathak, and J. Weber, "Investigation of the Heat Conduction in Axial Piston Pumps by Measurement and Simulation," in *IEE GFPS 2024*, Hurtigsval, Sweden, 2024.

[10] R. Ivantysyn, J. Weber, A. Kunze, and W. Uffrecht, "Thermal Analysis of the Cylinder Block of an Axial Piston Pump – The Key to Monitoring Efficiency," in *IFK2024*, 2024, pp. 1–21.

[11] R. Ivantysyn, W. Uffrecht, A. Kuntze, and J. Weber, "Efficiency Forecasting in Axial Piston Pumps : Leveraging High Speed Fluid Temperature Correlations for Condition Monitoring," in *JFPS*, Hiroshima, 2024, pp. 1–15.

[12] R. Ivantysyn and J. Weber, "Advancing Thermal Monitoring in Axial Piston Pumps : Simulation , Measurement , and Boundary Condition Analysis for Efficiency Enhancement," *International Journal of Fluid Power*, vol. 25, pp. 1–44, 2024, doi: 10.13052/ijfp1439-9776.2546.

Biographies

Roman Ivantysyn received the B.S. and M.S. degrees in Mechanical Engineering from Purdue University, West Lafayette, IN, USA. Since 2011, he has been a research assistant and Ph.D. candidate at the Chair of Fluid-Mechatronic Systems (LFD), TU Dresden, Germany, where his doctoral research addresses the thermal behavior of lubricating gaps in axial piston pumps with respect to efficiency and wear. His current research interests include large-scale mobile machinery and open-circuit displacement control, condition monitoring and lifetime studies of axial piston pumps, thermal analysis of pump systems, and surface shaping of hydrostatic bearings. Since 2024, he has also been CEO of Smart Hydraulic Solutions GmbH.